Multifractality in dilute magnetorheological fluids under an oscillating magnetic field

R. E. Moctezuma* and J. L. Arauz-Lara
Instituto de Física "Manuel Sandoval Vallarta," Universidad Autónoma de San Luis Potosí, Alvaro Obregón 64, 78000 San Luis Potosí, San Luis Potosí, Mexico

F. Donado
Instituto de Ciencias Básicas e Ingeniería de la Universidad Autónoma del Estado de Hidalgo-AAMF, Pachuca 42184, Pachuca, Mexico
(Received 11 June 2014; published 4 December 2014)

A study of the multifractal characteristics of the structure formed by magnetic particles in a dilute magnetorheological fluid is presented. A quasi-two-dimensional magnetorheological fluid sample is simultaneously subjected to a static magnetic field and a sinusoidal magnetic field transverse to each other. We analyzed the singularity spectrum $f(\alpha)$ and the generalized dimension $D(q)$ of the whole structure to characterize the distribution of the aggregates under several conditions of particle concentration, magnetic field intensities, and liquid viscosity. We also obtained the fractal dimension D_g, calculated from the radius of gyration of the chains, to describe the internal distribution of the particles. We present a thermodynamic interpretation of the multifractal analysis, and based on this, we discussed the characteristics of the structure formed by the particles and its relation with previous studies of the average chain length. We have found that this method is useful to quantitatively describe the structure of magnetorheological fluids, especially in systems with high particle concentration where the aggregates are more complex than simple chains or columns.

DOI: 10.1103/PhysRevE.90.062303 PACS number(s): 83.80.Gv, 05.45.Df, 61.43.Hv

I. INTRODUCTION

Objects having irregular forms or a complex mass distribution are commonly observed in nature, in man made materials, and in mathematical sets and functions [1]. These objects, that sometimes appear structureless, exhibit scaling properties having fractal or multifractal characteristics, which provide a good mathematical description of the physical processes in such materials. A multifractal system is an object that needs more than a single fractal dimension to describe its distribution, i.e., a discrete or continuous spectrum of exponents is needed [2]. Since the last century, fractals have been of mathematical, scientific, engineering, and purely artistic interest, and their mathematical language has been used as a powerful tool to characterize diverse systems in almost all science disciplines [3,4]. In physics, fractals have been used to study the kinetics and structure of disordered materials, such as polymers, colloids, aerosols, and gels [5–7]. They also have applications in numerous other areas, including transport phenomena, dynamics of random materials, the growth and form of complex patterns, hydrodynamic instabilities, etc. [8–10]. Moreover, fractal and multifractal concepts have been used to study systems as the bifurcating structure of trees, blood vessels, geochemical patterns, fractured surfaces of materials, music analysis, and galaxy distributions, among others [11–14]. It has been shown that fractals are of great utility as they may reflect the underlying physical process driving physical phenomena and they may act as diagnostics of anomalous behavior.

In this paper, we present a quantitative analysis of the geometry of the structures formed in a magnetorheological (MR) fluid in the presence of two different magnetic fields. In magnetorheological fluids, which are dispersions of micrometric magnetic particles in nonmagnetic liquids, when a static magnetic field is applied, aggregates are formed due to the magnetic moment induced in the particles [15–18]. These aggregates cause noticeable changes in the physical properties of the systems, and their characteristics depend mainly on the magnetic field intensity and particle concentration [19]. The study of the formed structure enables us to see a description of the physical properties of MR fluids, such as yield stress, viscosity, magnetization, and elastic modulus [20–22]. At low particle concentrations, the formation of chains is followed by the formation of thicker aggregates due to the coalescence of the chains. This system can be described as an ensemble of chains having an exponential distribution [23]. As we consider higher particle concentrations, the aggregates become more complex forming interconnected structures whose description in terms of chains and columns is insufficient. Some of the fractal and multifractal properties of this kind of structure have been previously studied [20,24–26]. However, a comprehensive study of the multifractal characteristics in a magnetic dispersion is carried out here.

When a sinusoidal magnetic field is applied in addition to the static field, the effective oscillating magnetic field drives the system to different configurations [19,27]. In Ref. [19], the average chain length for different values of frequency, particle concentration, viscosity, and magnetic field intensities was studied. In this paper, we use the same large collection of digital photographs obtained in that study to analyze the complexity of the different distributions of the aggregates within the sample and the distribution of the particles in a single chain or aggregate. For the former analysis, we use multifractal measurements, whereas for the latter we calculate the radius of gyration of the aggregates.

In Sec. II we briefly revise the scheme of the multifractal formalism. In Sec. III the multifractal characteristics of the distribution of the chains under several conditions in terms of

*rosario@ifisica.uaslp.mx

the singularity spectrum and the generalized fractal dimension are presented. Section IV shows the behavior of the fractal dimension determined by the relationship between the number of particles in single aggregates and its radius of gyration. The fractal dimension calculated in this way describes the distribution of the particles in the aggregate. In Sec. V we derive some thermodynamic quantities taking advantage of the formal relationship between the multifractal formalism and the equilibrium statistical mechanics approach. Finally, in Sec. VI we present the conclusions.

II. MULTIFRACTAL ANALYSIS

The fractal and multifractal characteristics of the system were measured by using IMAGEJ and its plugin FRACLAC [28]. This program is based on the box-counting method to obtain several quantities related to fractality. The method consists of covering the total region of study with boxes of equal size (l) and counting the number of boxes N that have at least one particle. Then, the size of the boxes is reduced, and the counting is repeated. The fractal dimension D_B is defined as the slope of a log-log graph of the number of boxes containing pixels and the inverse of the box size, that is, $N \approx (\frac{1}{l})^{D_B}$. To calculate the multifractal quantities, FRACLAC uses the multifractal formalism proposed by Chhabra *et al.* [29], Chhabra and Jensen [30], and Chhabra *et al.* [31] for determining the singularity spectrum $f(\alpha)$ directly from experimental data. According to this method $f(\alpha)$ is defined as

$$f(\alpha_q) = \frac{\sum_i \mu_i \ln \mu_i}{\ln l}, \tag{1}$$

where

$$\mu_i = \frac{P_i^q(l)}{\sum_i P_i^q(l)}, \tag{2}$$

and

$$\alpha = \frac{\sum_i \mu_i \ln P_i}{\ln l}, \tag{3}$$

where α is the singularity strength which quantifies the local degree of regularity, μ_i is the mean number of particles contained in the ith box with a certain size and position, P_i is the probability of finding the particles at the ith box, $f(\alpha)$ describes how densely the singularities are distributed, and q is the moment order of the measures of all boxes covering the distribution. For $q > 1$, $\mu_i(q)$ accentuates the importance of the more singular regions (denser regions) of the measure, whereas for $q < 1$ it accentuates the less singular regions (rarer regions), and for $q = 1$, $\mu_i(1)$ replicates the original measure [30]. If the graph of $f(\alpha)$ is humped, the object is considered multifractal. If the graph converges, the object is considered mono- or nonfractal.

The generalized dimension $D(q)$, representing a statistical description of how mass varies with l (box size) in an image, is defined as

$$D(q) = \frac{1}{(q-1)} \lim_{l \to 0} \frac{\ln \sum_i P_i^q(l)}{\ln(l)}. \tag{4}$$

The graph of $D(q)$ vs q is decreasing for multifractals but nondecreasing for mono- or nonfractals. The maximum value of $f(\alpha)$ corresponds to $D(0)$, which represents the box-counting dimension D_B.

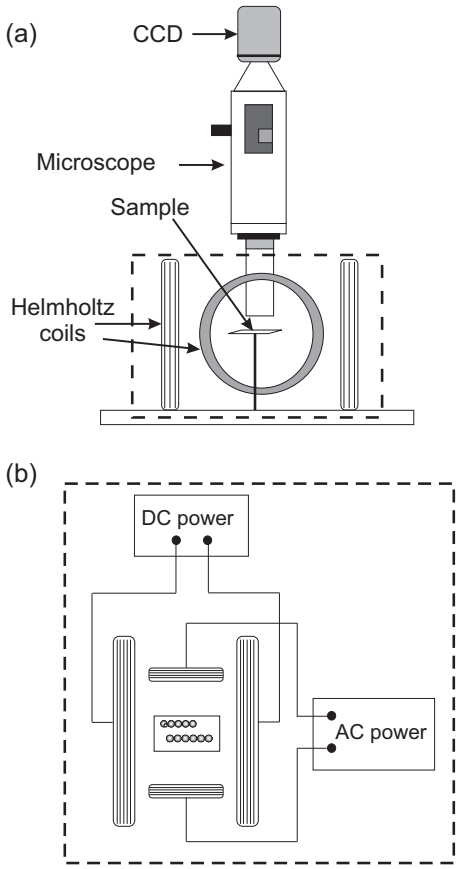

FIG. 1. Experimental setup. (a) A schematic side view and (b) a schematic top view.

III. EXPERIMENT

We study a MR fluid which is composed of mineral magnetite particles about 65 μm dispersed in dexron oil. The experimental setup is presented in Fig. 1. Briefly, a sample of the MR fluid is poured into a cell of 14 mm width and 17 mm length. The aggregation is observed using an optical microscope with a digital camera attached to it. We use two pairs of Helmholtz coils to generate two different magnetic fields: a static field and a sinusoidal field transverse to each other, both on the horizontal plane. Thus, the effective field oscillates on the x-y plane. We start the experiment with the particles dispersed in the oil and settled down at the bottom of the cell, then the fields are turned on. After 200 s the fields are turned off, and the final stage is recorded. We took a series of digital photographs at different stages under several conditions of particle concentration, liquid viscosity, and magnetic fields. From the photographs the multifractal analysis is performed.

We consider first the multifractal spectra for a series of samples where particle concentration is varied. The cases with and without perturbation are compared. In order to illustrate the kind of structures studied here, in Fig. 2 we show the distribution of the aggregates in a MR fluid sample for three different values of the particle area fraction ϕ_{2D}

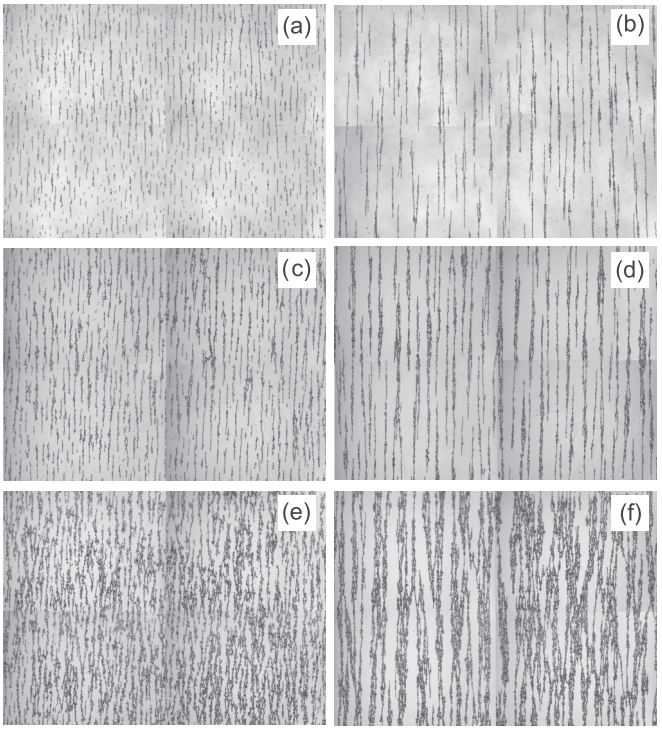

FIG. 2. MR structure formed in the presence of a static (92 G) magnetic field (first column) and in the presence of a static (80 G) and an oscillating (12 G) magnetic field (second column) at different area fractions: in (a) and (b) $\phi_{2D} = 0.076$, in (c) and (d) $\phi_{2D} = 0.128$, and in (e) and (f) $\phi_{2D} = 0.244$. The frequency of the oscillating field is 2 Hz, and the viscosity of the liquid is 76 cP.

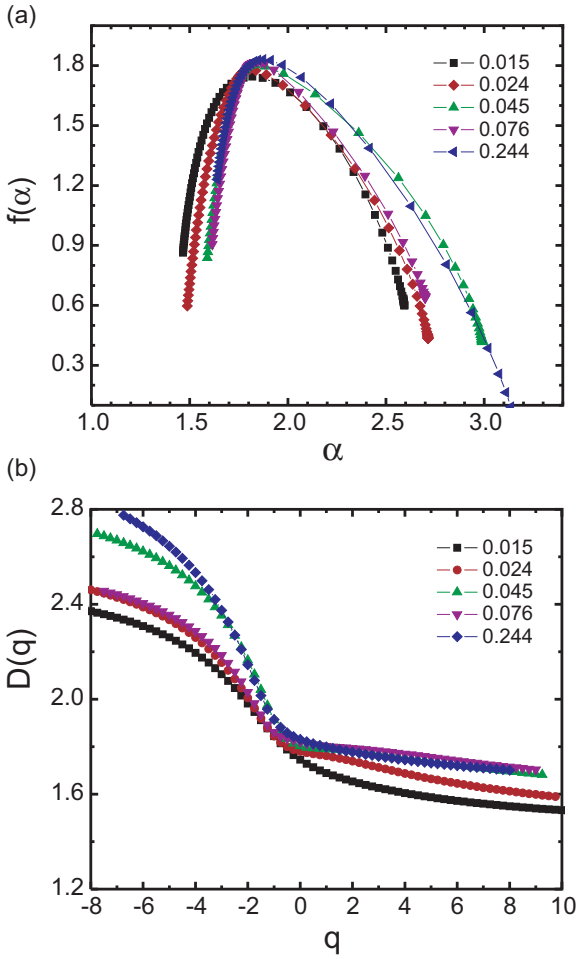

FIG. 3. (Color online) (a) Singularity spectrum $f(\alpha)$ and (b) generalized dimensions $D(q)$ of the MR fluid structure formed in the presence of a static magnetic field $H_c = 80$ G at different particle concentrations ϕ_{2D}.

for the case when only the static field is present (a), (c), and (e) and when both fields are present (b), (d), and (f). The singularity spectrum and the generalized dimensions for different particle concentrations when only the static field is applied are shown in Fig. 3. It can be seen that the singularity spectrum converges rapidly for lower values of α than for larger ones; this means that the denser regions have a lower degree of heterogeneity of the chain distribution, whereas the rarer ones are more heterogeneous [32]. The singularity spectra and the generalized dimensions for several particle concentrations are shown in Fig. 4 for the case when both fields are turned on. From Fig. 4(a), we can observe that the singularity spectrum is shifted to the right with increasing particle concentration. For $\phi_{2D} = 0.015$ and 0.024, the lower particle concentration samples, the spectra of fractal dimensions are wider, which implies a more complex distribution. From Fig. 4(b) it can be seen that all curves decrease as q increases, demonstrating the multifractal characteristic of the patterns. Comparing Figs. 3 and 4 it can be seen that a system subjected only to a static magnetic field exhibits less complexity in its structure than the systems subjected to both fields.

Figure 5 shows the box-counting fractal dimension (the higher value of the singularity spectrum) D_B as a function of ϕ_{2D}. It is observed that for all particle concentrations, D_B is higher when only the static magnetic field is applied than when both fields are applied. It is also observed that the change is slower when both fields are present. This is due to the fact that when only the static field is present, the chains fill the space more homogeneously than when both fields are present. From the graph we can observe that both curves show a tendency to grow as particle concentration increases. At low particle concentrations we can observe the formation of chains of different sizes dispersed across the sample. As particle concentration increases, the number of chains increases, forming interconnected structures which tend to fill the space in both directions. In this case, the system appears less complex due to the fact that the chains have a narrower distribution.

We also analyze the effect of the frequency of the sinusoidal field using a static field $H_c = 80$ G and a sinusoidal field $H_p = 12$ G. In Fig. 6 we depict (a) the graph of the singularity spectrum $f(\alpha)$ and (b) the generalized dimensions $D(q)$ for several frequencies for a system where $\phi_{2D} = 0.05$. As can be observed here, each curve decreases as a function of increasing q, demonstrating the multifractal characteristic of the patterns. The fractal dimension D_B is shown in Fig. 7 for all the frequencies studied here. It can be seen here that for low frequencies the distributions presents a minimum around 2 Hz. Although the differences between the values of D_B are small, they actually correspond to appreciable differences in

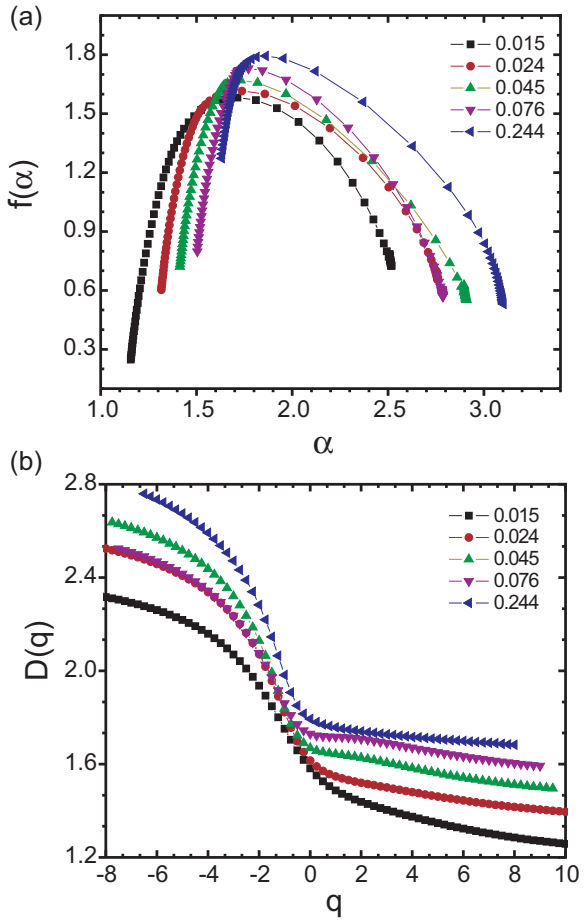

FIG. 4. (Color online) (a) Singularity spectrum $f(\alpha)$ and (b) generalized dimensions $D(q)$ of the MR fluid structure formed in the presence of both a static (80 G) and an oscillating magnetic field (12 G) at a frequency of 2 Hz at different particle concentrations ϕ_{2D}.

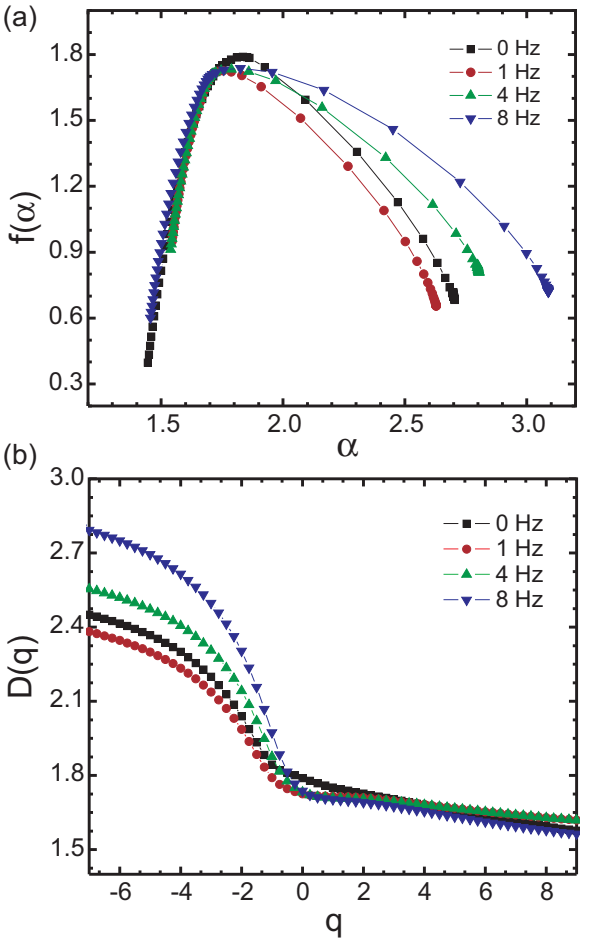

FIG. 6. (Color online) (a) Singularity spectrum $f(\alpha)$ and (b) generalized dimensions $D(q)$ of the MR fluid structure for different values of the frequency of the perturbation field. The magnitudes of the fields are as follows: $H_c = 80$ and $H_p = 12$ G, and $\phi_{2D} = 0.05$.

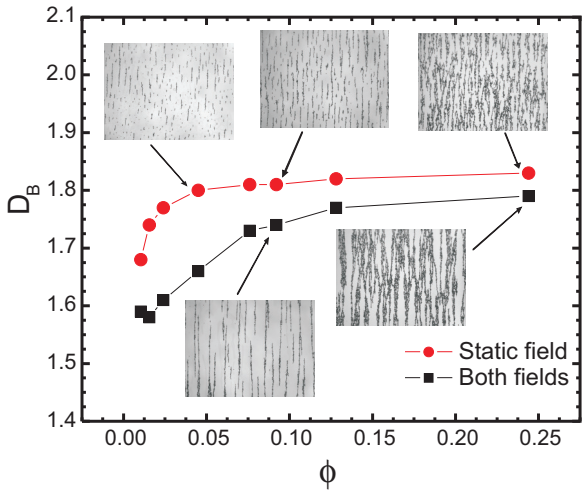

FIG. 5. (Color online) Box-counting fractal dimension of the MR fluid structure formed in the presence of a static magnetic field of 92 G (circles) and a static and oscillating magnetic field (squares) of 80 and 12 G, respectively, at different particle concentrations.

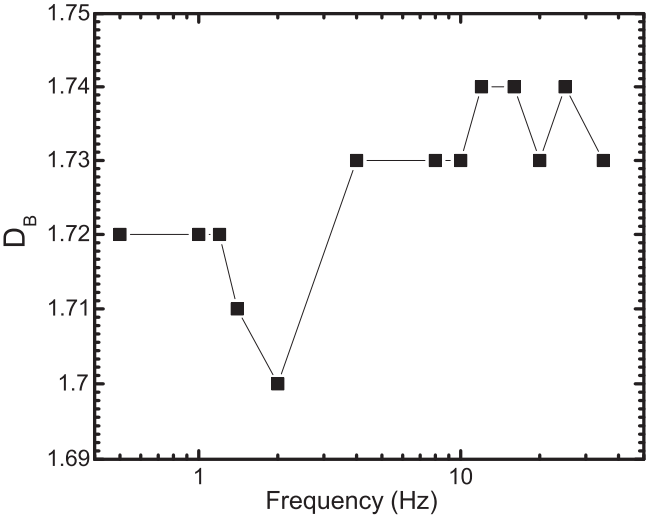

FIG. 7. Box-counting fractal dimension (D_B) of the MR fluid cluster at different frequencies of the oscillating field. The static field is fixed at 80 G, the oscillating field is fixed at 12 G, and $\phi_{2D} = 0.05$.

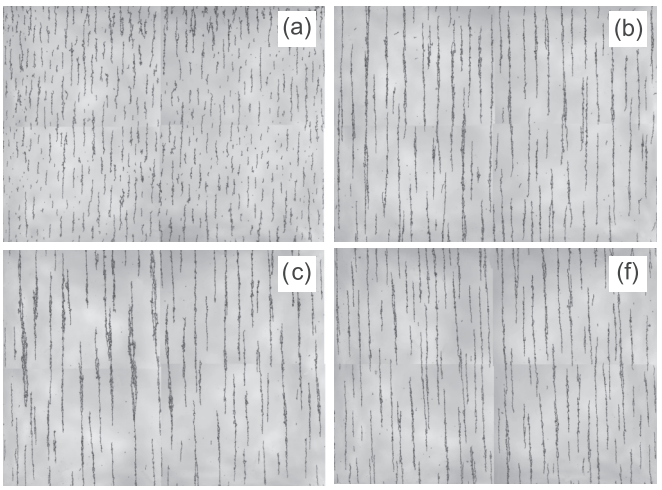

FIG. 8. MR fluid structure for different values of the frequency of the perturbation field: (a) 0, (b) 1, (c) 2, and (d) 10 Hz. The applied fields are as follows: $H_c = 80$ and $H_p = 12$ G. The viscosity of the liquid is 76 cP and $\phi_{2D} = 0.05$.

the structure of the system. This is illustrated in Fig. 8 where the final configuration of the MR fluid at different frequencies is shown. As one can see here, the structure formed at 2 Hz, corresponding to a lower D_B, Fig. 8(c), is less spread than those formed at other frequencies. This is in accord with previous reports that the changes in the average chain length present a critical behavior around a frequency of 2 Hz [19,33]. For frequencies below 2 Hz, the average chain length $\bar{L}$ increases with frequency, whereas for frequencies greater than 2 Hz it decreases with increasing frequency. This behavior is also reflected in the specific viscosity of the fluid: For frequencies under 2 Hz, the viscosity increases with frequency, whereas for frequencies over 2 Hz the viscosity decreases with increasing frequency [19,33]. Comparing those results with the behavior of the fractal dimension, we observed that the critical behavior is related to the condition where the structure has smaller fractal dimension.

The singularity spectrum is also obtained in the case when both the static and the oscillating fields are varied keeping $H_p = 0.15H_c$. In Fig. 9(a) we show the maximum value of the spectrum D_B as a function of the static magnetic field. As we can see, there are little differences as the magnetic field increases. The behavior of the system as a function of the viscosity of the oil where the particles are dispersed is shown in Fig. 9(b). Here, one can observe that at low viscosities the fractal dimension changes. However, for higher viscosities, D_B remains almost the same. This behavior arises since, at higher viscosities, the aggregation process is very slow due to higher drag forces overdamping the motion. At low viscosities the aggregation is faster, and the distribution of the chains is more complex.

The width of the $f(\alpha)$ spectrum $\Delta = \alpha_{\max} - \alpha_{\min}$ can be used to indicate the complexity of a structure: Monofractal structures give narrow spectra, whereas multifractal distributions give broader spectra [34,35]. The degree of multifractality of the structures in MR fluids for different (a) particle concentrations and different (b) frequencies is shown

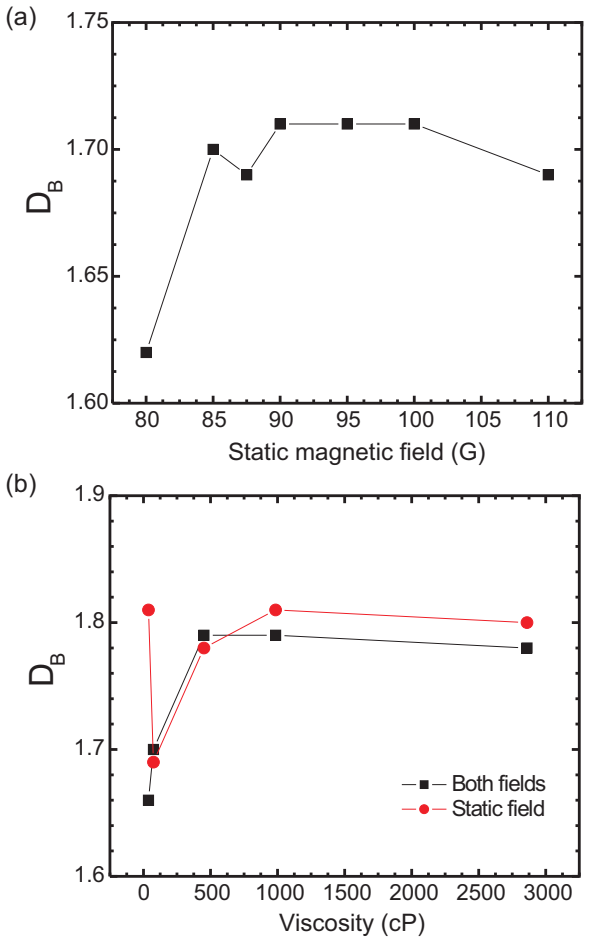

FIG. 9. (Color online) Box-counting fractal dimension of the pattern formed (a) at different magnitudes of the magnetic fields. The magnitude of the oscillating field is $H_p = 0.15H_c$ and (b) at different values of the viscosity.

in Table I. Here, we have the width of the singularity spectrum for the positive values of the q's exponents as these are characteristic of the densely populated measures. From Table I(a) we can see that Δ is greater for low concentrations than for high concentrations and that it is greater when the system is subjected to both magnetic fields than when there

TABLE I. Width of $f(\alpha)$ for MR fluids: (a) at different particle concentrations ϕ_{2D} in the presence of a static magnetic field H_c and with both fields (H_p at a frequency of 2 Hz) and (b) at different frequencies of H_p at $\phi_{2D} = 0.05$.

(a)			(b)	
ϕ_{2D}	$\Delta(H_c)$	$\Delta(H_c + H_p)$	Hz	Δ
0.015	0.22	0.33	0.0	0.21
0.024	0.19	0.22	0.3	0.18
0.045	0.12	0.17	0.5	0.16
0.076	0.12	0.14	1.0	0.11
0.092	0.11	0.13	1.4	0.16
0.128	0.09	0.14	8.0	0.17
0.244	0.13	0.11	25	0.14

is only the static field applied. This indicates that the particle concentration and the nature of the effective magnetic field are directly related to the width of the curve which increases when concentration decreases. From Table I(b) we can see that the value of Δ does not vary too much for the different frequencies of the perturbation field.

IV. RADIUS OF GYRATION AND ITS FRACTAL DIMENSION

The multifractal analysis presented in the previous section provides a measure of the complexity of the distribution of chains in a sample of MR fluid. Another important measurement is related to how the particles are distributed in a single chain or aggregate. One way to characterize such distribution is by measuring the radius of gyration R_g of each chain in a sample for different conditions. In a chain containing N particles, the radius of gyration is given by [2,36]

$$R_g^2 \equiv \frac{1}{N}\sum_{i=1}^{N}(\vec{R}_i - \vec{R}_{\text{c.m.}})^2. \tag{5}$$

Here $\vec{R}_i$ is the position of each particle, and $\vec{R}_{\text{c.m.}}$ is the position of the center of mass of the aggregate. The radius of gyration gives us information about the way the particles are distributed in a chain of a certain size. The radius of gyration as a function of the number of particles follows a power law given by [36,37]

$$R_g(N) \sim N^{1/D_g}, \tag{6}$$

where D_g is the fractal dimension. In practice, a simple way to calculate the radius of gyration is performed by taking the positions of the pixels within the chain, instead of resolving single particles in a chain.

Figures 10 and 11 show R_g vs N for two different samples, one with $\phi_{2D} = 0.015$ and the other with $\phi_{2D} = 0.244$, respectively. The fractal dimension for the lower concentration is $D_g = 1.16$ and for the higher concentration is $D_g = 1.78$. Thus, the fractal dimension approaches 1 for low particle concentration samples since the aggregates formed are chains. For higher particle concentrations, D_g approaches 2 due to the fact that the typical structures formed here are aggregates of chains which cover an area instead of defining a line.

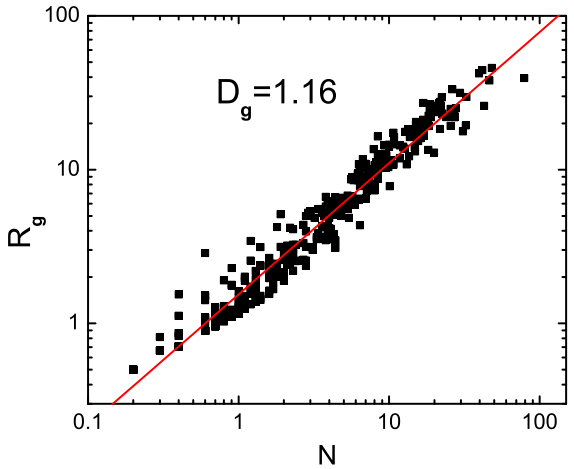

FIG. 10. (Color online) Radius of gyration R_g vs number of particles N in a MR fluid with $\phi_{2D} = 0.015$.

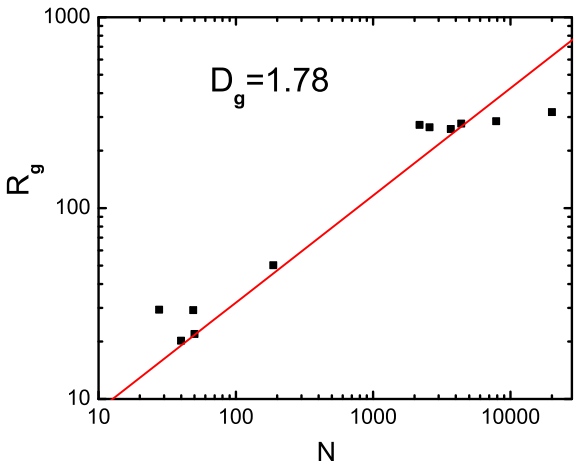

FIG. 11. (Color online) Radius of gyration (R_g) vs number of particles (N) in a MR fluid with $\phi_{2D} = 0.244$.

Figure 12 shows different aggregates formed in the MR fluid samples and their fractal dimension D_g calculated through Eq. (6). The fractal dimension approaches 1 for samples containing short and large chains. For samples containing small clusters D_g increases (1.34), and for samples containing big clusters it approaches 2.

Figure 13 shows the fractal dimension, calculated from Eq. (6) for all cases studied above. In the case of the variation in particle concentration (a), we observe a wider range of values of the fractal dimension. This behavior derives from the fact that aggregates go from chainlike to more complex structures formed by the aggregation of chains, forming more extended clusters which tend to fill the space, leading to values of the fractal dimension closer to 2. In the same Fig. 13(a), we compare the case when only the static magnetic field is turned on with the case when both fields are turned on. At low

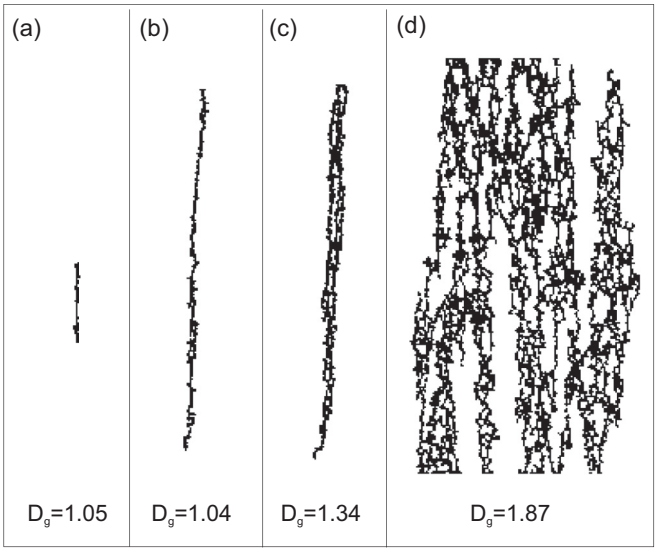

FIG. 12. (a) Short chain, (b) large chain, (c) small cluster, and (d) big cluster formed in the MR fluid samples at different conditions.

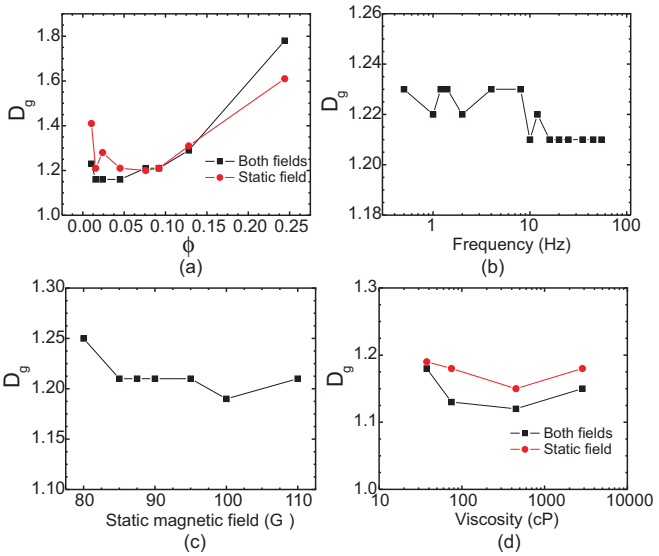

FIG. 13. (Color online) Fractal dimension estimated from the radius of gyration and the size of the clusters for different values of (a) particle concentration, (b) frequency, (c) magnitude of the magnetic fields, and (d) viscosity.

particle concentration the values of the fractal dimension are small since chains are the more populated kinds of structures.

In the case of the variation in frequency we found that at lower frequencies the fractal dimension decreases as frequency increases, Fig. 13(b). This is in accord with observations indicating that oscillation favors aggregation, thus the system goes from a state of numerous short chains to a state of less but larger chains. At high frequencies the differences when frequency changes are not noticeable because the oscillating field loses its effectiveness to rearrange the chains, i.e., these do not respond anymore. The general behavior of the fractal dimension as a function of the magnetic field shows a certain tendency to decrease as the magnetic field increases, Fig. 13(c). It is likely that this behavior is due to the formation of larger chains that arise by increasing the magnetic field when the samples are in the lower concentration regime. The general behavior when the viscosity is varied is shown in Fig. 13(d). For high viscosity the aggregation is more difficult, and the more numerous kinds of structures are short chains. Only at low viscosities is there the possibility to obtain aggregation of chains.

V. THERMODYNAMIC INTERPRETATION OF THE MULTIFRACTAL MEASURES

There is a formal connection of the multifractal formalism with that of equilibrium statistical mechanics. Therefore, we can evaluate thermodynamic quantities via this formalism [29,31,38]. If a sample, i.e., a photograph from a experiment, is covered with boxes of size l having a probability $P_i(l)$, the partition function for equal box sizes is given by

$$Z(q) = \frac{\sum_i P_i^q(l)}{l^\tau}. \tag{7}$$

We can equate this partition function to unity without losing generality [31,32], i.e.,

$$Z(q) = \sum_i P_i^q(l) \sim l^\tau. \tag{8}$$

On the other hand, the canonical partition function of a mechanical system is the sum of the Boltzmann factors $e^{-\beta E_i}$, where β is the inverse temperature. Thus, defining in our system $E_i = -\ln(P_i)$, we can write

$$Z(\beta) \equiv \sum_i e^{-\beta E_i} = \sum_i e^{[q\ \ln(P_i)]}. \tag{9}$$

Thus we can identify q as the Boltzmann temperature $\beta = 1/kT$ and E_i as the energy of the ith box. An alternative formulation for the partition function is in terms of an exponential of n times the free energy,

$$Z(\beta) \equiv e^{[-nF(\beta)]} = e^{[-\tau\ \ln(l)]}, \tag{10}$$

where β is absorbed in the free energy [39]. Here, we can identify the mass exponent function $\tau(q)$ with the free energy. Moreover, $f(\alpha)$ is related to $\tau(q) = (q-1)D(q)$ by a Legendre transformation when $f(\alpha)$ and $D(q)$ are smooth functions of α and q, respectively. Then, we can identify the curve of $f(\alpha)$ as an entropy vs internal energy α of a statistical mechanical system [30].

In the method of Chhabra *et al.*, a direct computation of $f(\alpha)$ is possible if the weighting term used to compute the Hausdorff dimension and the singularity strength is μ_i [Eq. (2)], which plays the role of the Boltzmann factor in thermodynamics, i.e.,

$$\mu_i(q,l) = \frac{[P_i(l)]^q}{\sum_i [P_i]^q} = \frac{e^{-\beta E_i(l)}}{\sum_j e^{-\beta E_j(l)}}. \tag{11}$$

In this sense, the singularity spectra, obtained for the different conditions studied here, can be interpreted as the entropy of the system as a function of the internal energy [Figs. 3(a), 4(a), and 5(a)]. The left side of the curve indicates that the entropy increases when the internal energy increases. This means that at $f(\alpha) = D_B$ the system reaches its more stable configuration where the energy is distributed uniformly within the sample. Furthermore, the behavior of the singular spectra in Fig. 4(a) shows that, for low particle concentrations, a local minimum of energy is reached slower than for high concentrations and it is reached at smaller values of the internal energy and entropy. At high particle concentrations the entropy is higher, indicating that this could be a more stable state. However, when only the static field is applied [Fig. 3(b)], the changes in entropy of the system are similar for the different concentrations studied here. If we increase particle concentration in a system with only the static field applied, Fig. 3(a), we could reproduce the same behavior of Fig. 4(a). On the other hand, for the frequencies studied here, the most probable configuration of the aggregates experiences small changes (Fig. 6).

The mass exponent function $\tau(q)$ is a straight line for mono- or nonfractal objects. Thus, a deviation from linearity reveals some degree of multifractality and nonlinearity of a pattern. Figure 14 shows $\tau(q)$ vs q for five different particle concentrations when only the static field is on (a) and when

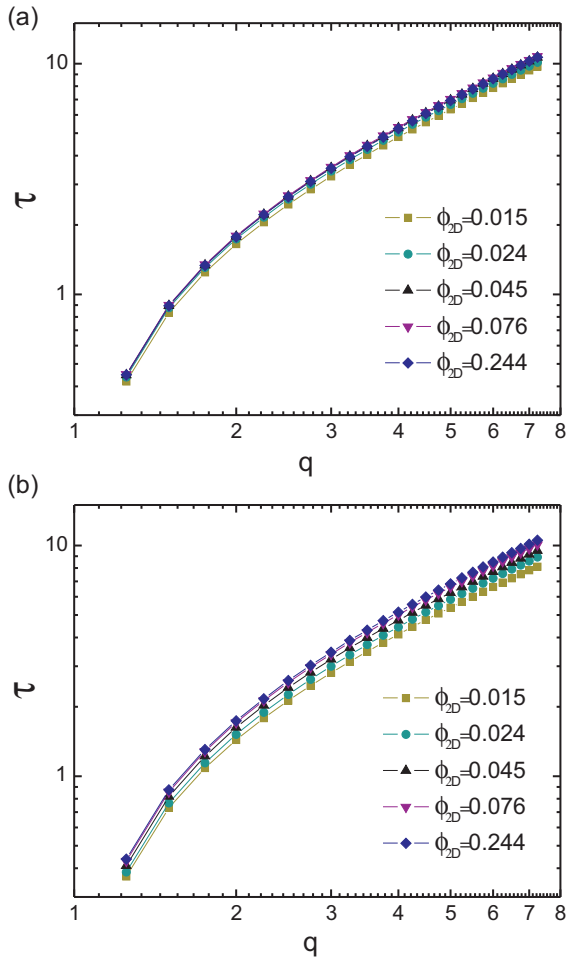

FIG. 14. (Color online) Free energy $\tau(q)$ vs inverse of temperature for different particle concentrations of the MR fluid: (a) in the presence of a static magnetic field $H_c = 80$ G and (b) in presence of static ($H_c = 80$ G) and oscillating ($H_p = 12$ G) magnetic fields.

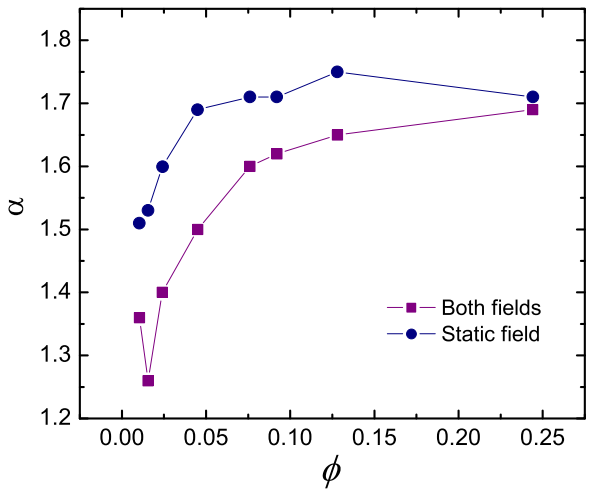

FIG. 15. (Color online) Lipschitz-Hölder exponent (internal energy) vs particle concentration of the MR fluid.

both fields are turned on (b). From the graph we can observe that there is not a single slope characterizing the distribution. If we interpret this curve as the free energy, we can say that the available energy to carry out the thermodynamic work in these systems increases with particle concentration and as temperature decreases (temperature decreases as q increases since $q = \beta$). Comparing Figs. 14(a) and 14(b) we can observe that the configuration of the system, subjected only to the static field, forms similar structures, whereas the system with both fields exhibits more evident differences. In Fig. 15 we depicted the slope α of $\tau(q)$ for positive values of q, which is interpreted as the internal energy. From the figure it can be seen that the internal energy in the MR fluid systems increases with particle concentration and it presents lower values for the case when only the static field is applied.

VI. COMMENTS AND REMARKS

We have studied the multifractal characteristics of the aggregates formed by the magnetic particles in magnetorheological fluids under an effective oscillating magnetic field. We vary different parameters, such as frequency, particle concentration, magnitude of the magnetic fields, and viscosity. The singularity spectrum and generalized dimensions make evident the multifractal behavior in MR fluids subjected to two different magnetic fields.

It was observed that, when only the static field is applied, the chains are distributed homogeneously along the whole sample and it occurred for the different concentrations studied here. However, when both fields are applied, the configuration changes drastically, and the particle distribution becomes inhomogeneous. All these features can actually be appreciated by visual inspection of the system's pictures. However, for a quantitative characterization of the different properties we need to resort to a theoretical analysis. As we show here, the multifractal analysis provides a theoretical tool which allows us the characterization of the system's structure as a whole. This analysis is complementary to previous papers where the main objective was the description of single chains. The multifractal method describes the system at length instead of describing it as a distribution of individual chains or columns. Combining the multifractal analysis for the whole structure and the analysis through the radius of gyration for the distribution of particles within each structure, we obtain a complete description of the complex structures formed by the particles.

From the formal relation with statistical mechanics, we observed that the distribution always evolves toward configurations of minimum energy and maximum entropy.

ACKNOWLEDGMENTS

Partial financial support from CONACyT, (Mexico) through Grants No. 80629 and No. 182132 and the postdoctoral fellowship to R. E. Moctezuma by Red Temática de Materia Condensada Blanda are acknowledged. We thank A. Ramírez-Saito for providing technical support.

[1] B. B. Mandelbrot, in *The Fractal Geometry of Nature* (W. H. Freeman, New York, 1982), 468p.

[2] T. G. Dewey, *Fractals in Molecular Biophysics* (Oxford University Press, New York, 1997).

[3] Z. Q. Jiang and W. X. Zhou, Physica A **387**, 4881 (2008).

[4] R. E. Moctezuma, J. L. Carrillo, and M. E. Mendoza, Integr. Ferroelectr. **111**, 88 (2009).

[5] R. C. Ball, Physica D **38**, 13 (1989).

[6] M. M. O. Eleya, S. Ko, and S. Gunasekaram, Food Hydrocolloids **18**, 315 (2004).

[7] H. K. Janssen and O. Stenull, Phys. Rev. E **85**, 051126 (2012).

[8] G. Guyon, C. D. Mitescu, J. P. Hulin, and S. Roux, Physica D **38**, 172 (1989).

[9] E. C. Herrera-Hernández, M. Coronado, and H. Hernández-Coronado, Phys. Rev. E **88**, 063004 (2013).

[10] A. S. Balankin and B. E. Elizarraraz, Phys. Rev. E **85**, 025302(R) (2012).

[11] A. Panahi and Q. Cheng, Math. Geol. **36**, 827 (2004).

[12] V. S. Deviha, P. Rengarajan, and R. J. Hussain, Appl. Math. Sci. **7**, 527 (2013).

[13] K. J. Hsu and A. J. Hsu, Proc. Natl. Acad. Sci. USA **87**, 938 (1990).

[14] P. J. E. Peebles, Physica D **38**, 273 (1989).

[15] L. J. Felicia and J. Philip, Phys. Rev. E **89**, 022310 (2014).

[16] J. de Vicente, D. J. Klingenberg, and R. Hidalgo-Alvarez, Soft Matter **7**, 3701 (2011).

[17] I. Arief and P. K. Mukhopadhyay, J. Magn. Magn. Mater. **360**, 104 (2014).

[18] K. Shahrivar and J. de Vicente, Smart Mater. Struct. **23**, 025012 (2014).

[19] F. Donado, U. Sandoval, and J. L. Carrillo, Phys. Rev. E **79**, 011406 (2009).

[20] J. L. Carrillo, F. Donado, and M. E. Mendoza, Phys. Rev. E **68**, 061509 (2003).

[21] J. L. Carrillo, M. E. Mendoza, and F. Donado, J. Stat. Mech.: Theor. Exp. (2005) P06001.

[22] J. Rodríguez-López, L. Elvira, P. Resa and F. Montero de Espinosa, J. Phys. D: Appl. Phys. **46**, 065001 (2013).

[23] R. Agustín-Serrano, F. Donado, and E. Rubio-Rosas, J. Magn. Magn. Mater. **335**, 149 (2013).

[24] E. M. de la Calleja Mora, J. L. Carrillo, M. E. Mendoza, and F. Donado, Eur. Phys. J. B **86**, 126 (2013).

[25] F. Martinez-Pedrero, M. Tirado-Miranda, A. Schmitt, F. Vereda, and J. Callejas-Fernandez, Colloids Surf., A **306**, 158 (2007).

[26] P. Domínguez-García, S. Melle, and M. A. Rubio, J. Colloid Interface Sci. **333**, 221 (2009).

[27] R. E. Moctezuma, F. Donado, and J. L. Arauz-Lara, Phys. Rev. E **88**, 032305 (2013).

[28] W. S. Rasband, IMAGEJ (U.S. National Institutes of Health, Bethesda, MD, 1997).

[29] A. B. Chhabra, C. Meneveau, R. V. Jensen, and K. R. Sreenivasan, Phys. Rev. A **40**, 5284 (1989).

[30] A. Chhabra and R. V. Jensen, Phys. Rev. Lett. **62**, 1327 (1989).

[31] A. B. Chhabra, R. V. Jensen, and K. R. Sreenivasan, Phys. Rev. A **40**, 4593 (1989).

[32] T. C. Halsey, M. H. Jensen, L. P. Kadanoff, I. Procaccia, and B. I. Shraiman, Phys. Rev. A **33**, 1141 (1986).

[33] U. Sandoval, J. L. Carrillo, and F. Donado, Rev. Mex. Fis. E **56**, 123 (2010).

[34] Z. Moktadir, M. Kraft, and H. Wensink, Physica A **387**, 2083 (2008).

[35] A. Szczepaniak and W. M. Macek, Nonlin. Processes Geophys. **15**, 615 (2008).

[36] J. Byrom and S. L. Biswal, Soft Matter **9**, 9167 (2013).

[37] D. Stauffer and A. Aharony, *Introduction to Percolation Theory*, 2nd ed. (Taylor & Francis, Philadelphia, 2003).

[38] T. Tél, Z. Naturforsch. **43A**, 1154 (1988).

[39] M. J. Feigenbaum, J. Stat. Phys. **46**, 919 (1987).